

Persistent shift of the Arctic polar vortex towards the Eurasian continent in recent decades

Jiankai Zhang¹, Wenshou Tian^{1*}, Martyn P. Chipperfield², Fei Xie³ and Jinlong Huang¹

The wintertime Arctic stratospheric polar vortex has weakened over the past three decades, and consequently cold surface air from high latitudes is now more likely to move into the middle latitudes^{1–5}. However, it is not known if the location of the polar vortex has also experienced a persistent change in response to Arctic climate change and whether any changes in the vortex position have implications for the climate system. Here, through the analysis of various data sets and model simulations, we show that the Arctic polar vortex shifted persistently towards the Eurasian continent and away from North America in February over the past three decades. This shift is found to be closely related to the enhanced zonal wavenumber-1 waves in response to Arctic sea-ice loss, particularly over the Barents–Kara seas (BKS). Increased snow cover over the Eurasian continent may also have contributed to the shift. Our analysis reveals that the vortex shift induces cooling over some parts of the Eurasian continent and North America which partly offsets the tropospheric climate warming there in the past three decades. The potential vortex shift in response to persistent sea-ice loss in the future^{6,7}, and its associated climatic impact, deserve attention to better constrain future climate changes.

A growing number of studies have examined the variability of the Arctic stratospheric polar vortex (hereafter, ‘polar vortex’, unless otherwise stated) in response to ‘Arctic amplification’^{3,8} associated with global warming, especially high-latitude sea-ice loss^{9,10}. Previous studies have found that the sea-ice loss, particularly over the BKS, would force the Arctic Oscillation (AO) or the Northern Annular Mode (NAM) into its negative phase during January and February^{11–14}, and that the sea-ice loss has weakened the polar vortex over the past decades^{11,13}. It was also reported that sea-ice loss over Arctic regions can lead to a cooler and stronger polar vortex, and thereby more stratospheric ozone loss during spring^{15–17}. However, most previous studies focused on the effects of climate warming on the strength of the polar vortex. Whether the position of the polar vortex is undergoing a persistent change in response to the climate warming has rarely been discussed. It is known that changes in the position of the polar vortex associated with vortex displacement events on short timescales can have a significant impact on stratosphere–troposphere coupling¹⁸, and even on mid- and high-latitude surface temperature¹⁹, sea-level pressure^{19,20} and the ocean system²¹. On the other hand, the trends in the wintertime surface temperature at northern high and mid-latitudes over the past three decades exhibit a zonally asymmetric feature— that is, there is a dramatic cooling over the Eurasian continent, but a rapid warming over the Arctic region and northeastern Canada²².

Whether this zonally asymmetric temperature trend is an indication of a position change of the polar vortex is an important question to address. In this study, the long-term change in the position of the polar vortex and its associated climatic effects are examined.

Figure 1 shows that since the 1980s the polar vortex in late winter (February) exhibits a persistent shift towards the Eurasian continent and away from North America, associated with significantly positive trends in potential vorticity (PV) over the Eurasian continent, but negative PV trends over Baffin Island. The December–February (DJF) mean position of the polar vortex and the PV trend are similar to those for February, although the shift of the polar vortex is not as significant as that in February. It should be noted that the monthly mean of daily vortex edge derived from the PV field is very similar to the monthly mean vortex edge (Supplementary Fig. 1), since the radiative heating in the polar lower stratosphere is very weak during winter and the PV field is approximately conserved on a monthly timescale. However, there are evident decadal oscillations in the position of the polar vortex in December and January, suggesting that the polar vortex has not experienced a persistent shift in these two months during the past three decades (Supplementary Fig. 1). The above analysis indicates that the changes in vortex position during February dominate the changes in DJF mean vortex location. The corresponding results derived from the MERRA reanalysis data are similar to those from the ERA-Interim data (Supplementary Fig. 1).

Figure 1d,e shows that the February mean of the polar vortex area covering the Eurasian continent increases significantly for the period 1980–2015, whereas the area over North America decreases. These fractional area changes are consistent with the shift of the polar vortex edge towards the Eurasian continent and away from North America shown in Fig. 1a. Also note that the DJF mean vortex area shows a significant positive trend over the Eurasian continent, but a negative trend over North America. In addition, the centre of the polar vortex (see Methods) is more likely to be located at lower latitudes between 0–100° E in February during the 2000s than before (Supplementary Fig. 2), further confirming that the polar vortex is shifting, as a whole, towards the Eurasian continent over the recent decades. Both ERA-Interim and MERRA data sets show that the February and DJF mean of vortex centre during the 2000s shifts further towards the Eurasian continent than before, although the locations of the vortex centre in ERA data are different from those in MERRA data (Supplementary Fig. 1).

As previous studies have reported that long-term changes in the strength of the polar vortex are related to sea-ice loss^{1,13,14}, it is worthwhile first examining whether the vortex shift is also caused by the sea-ice loss. Figure 2a shows that the BKS have lost significant

¹Key Laboratory for Semi-Arid Climate Change of the Ministry of Education, College of Atmospheric Sciences, Lanzhou University, Lanzhou 730000, China. ²School of Earth and Environment, University of Leeds, Leeds LS2 9JT, UK. ³College of Global Change and Earth System Science, Beijing Normal University, Beijing 100875, China. *e-mail: wstian@lzu.edu.cn

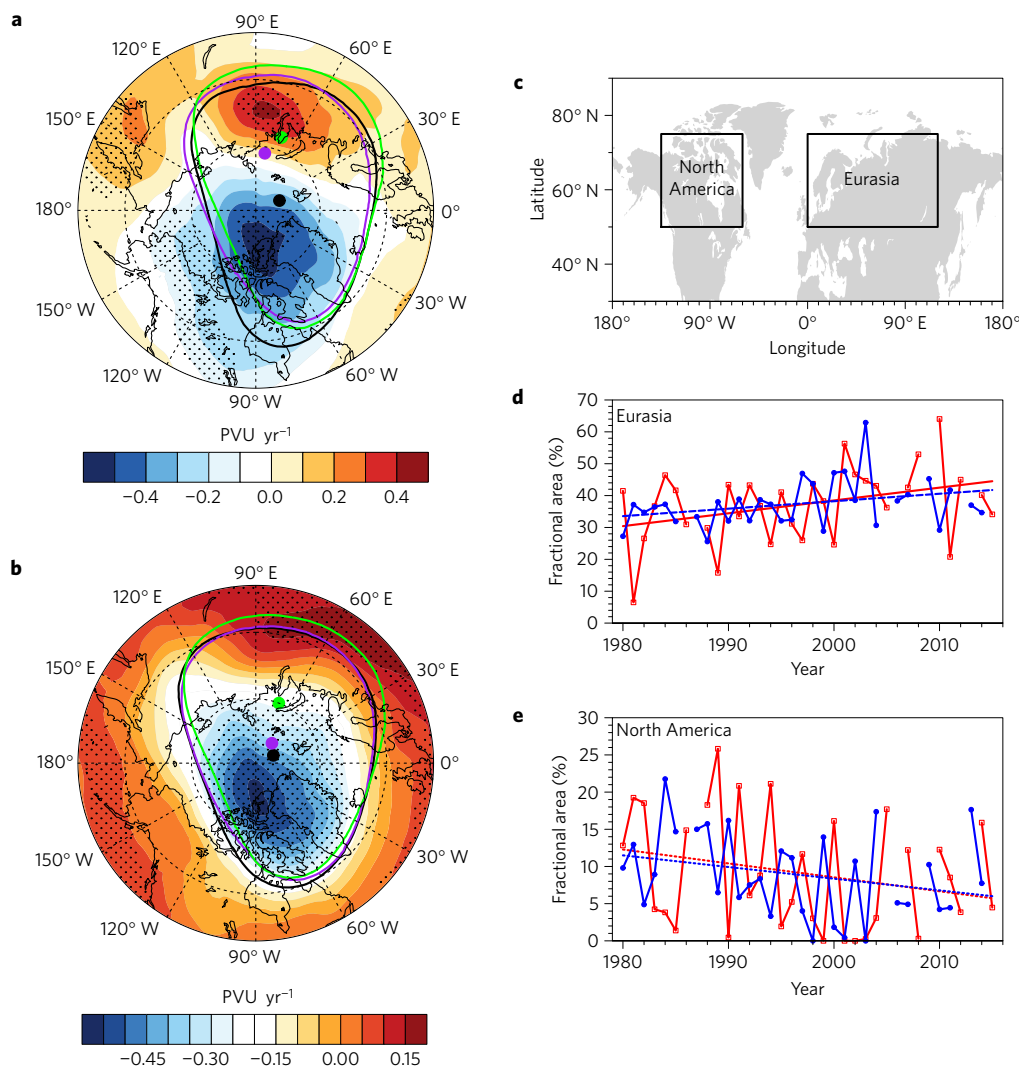


Figure 1 | Polar vortex position and fractional area of regions covered by the polar vortex. a,b, Decadal mean of vortex edge (coloured contour lines) and vortex centre (coloured dots) in the 1980s (black), 1990s (purple) and 2000s (green) as well as the PV trends (colour-filled contours) for the period 1980–2009, derived from ERA-Interim monthly data, averaged between the isentropic layers 430–600 K during February (**a**) and December–February (DJF) (**b**). **c,** The geographical regions of two key weather regimes indicated by the black boxes, that is, Eurasia and North America. **d,e,** Time series of fractional areas of the geographical regions in **c** covered by the polar vortex over the Eurasian continent and North America during February (red) and DJF mean (blue). The fractional area is defined as the area of the vortex which covers a region divided by the total area of the polar vortex. The trends over the dotted regions in **a,b** are statistically significant at the 90% confidence level according to the Student's *t*-test. Solid and dashed lines in **d,e** represent the corresponding linear trends which are statistically significant at the 95% and 90% confidence levels, respectively, whereas the linear trends denoted by the dotted lines are not significant at the 90% confidence level. The values of percentage area in February 1987, 2006, 2009 and 2013 are not calculated because the polar vortex broke up and its shape was distorted in these months (see Methods).

areas of sea-ice concentration (SIC) during autumn and winter in the 2000s. Here, we perform a composite analysis based on the SIC anomalies over the BKS (see Methods) to analyse the influence of SIC on the polar vortex. Figure 2b shows that there is larger PV over the Eurasian continent and smaller PV over North America during the low-SIC years than during the high-SIC years. This feature is in accord with the shift of the polar vortex towards the Eurasian continent and away from North America. To gain more insight into the effect of the SIC on the polar vortex, two WACCM climate model simulations (run R1 and R2) were performed with the same model configuration but with different SIC fields (see Methods). The SIC fields in runs R1 and R2 are representative of conditions during the 1980s and 2000s, respectively. The simulations successfully reproduce the higher PV values over the Eurasian continent and the lower PV values over Baffin Island in R2 than those in R1 during February (Fig. 2c). The polar vortex edge also shows a significant

shift towards the Eurasian continent. Results from two additional 60-year ensemble experiments (R3 and R4, see Methods), which are designed for detecting the influence of BKS sea-ice loss on the polar vortex shift, also show that the polar vortex shifts towards the Eurasian continent and away from North America (Supplementary Fig. 3). This analysis suggests that the sea-ice loss over the BKS in autumn and winter makes a large contribution to the vortex shift towards the Eurasian continent.

The enhanced heat flux associated with the loss of sea ice¹ warms the middle and lower troposphere (Supplementary Fig. 4a,b); however, the temperature in the upper troposphere and lower stratosphere (UTLS) is reduced (Supplementary Fig. 4c,d), corresponding to a baroclinic temperature structure. In conjunction with the warming of the Arctic troposphere, there are positive height anomalies at 850 hPa in both the reanalysis data and WACCM simulations (Fig. 3a,b), whereas the height at 50 hPa shows negative

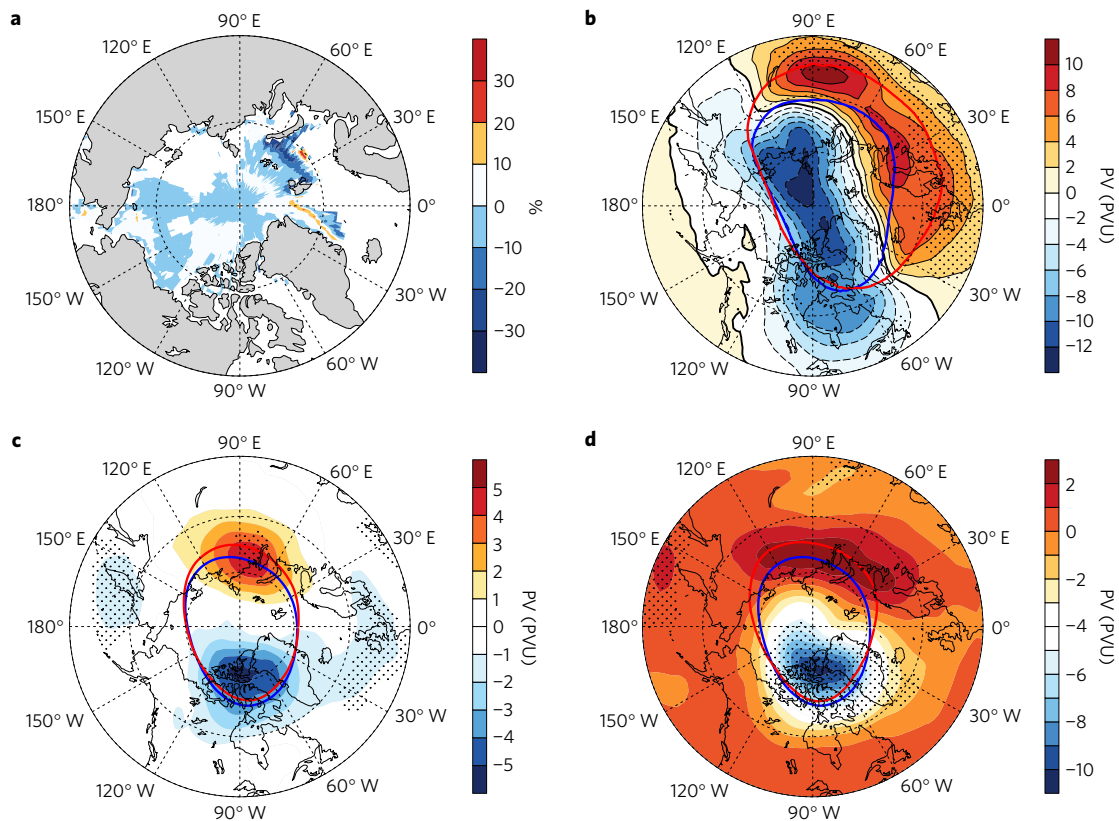


Figure 2 | Polar vortex shifts associated with the sea-ice loss. **a**, Differences in 6-month (September–February) mean SIC over the northern polar cap between the 2000s and the 1980s derived from the Hadley Centre Sea Ice data set. **b**, Composites mean differences in February mean PV between the Barents–Kara (BKS) low- and high-SIC years averaged between the isentropic layers 430–600 K. The February mean vortex edges during the BKS low-SIC years (red line) and high-SIC years (blue line) are also shown. **c**, Difference in February mean PV between model simulations (see Methods) R2 and R1 and February mean vortex edge in R1 (blue line) and R2 (red line) averaged between the isentropic layers 430–600 K. **d**, Difference in February mean PV between simulations R5 and R1 and February mean vortex edge in R1 (blue line) and R5 (red line) averaged between the isentropic layer 430–600 K. The differences over the dotted regions are statistically significant at the 90% confidence level according to the Student's *t*-test.

anomalies in response to the cooling in the UTLS in the low-SIC years (Fig. 3c,d). The baroclinic structure with a westward tilt with height is more noticeable in the height–longitude cross-section of height anomalies along 60° N (Fig. 3e,f and Supplementary Fig. 5c). Although there are some discrepancies between the modelled geopotential height anomalies and corresponding reanalysis results, both composite analysis and numerical results indicate that the forced height anomalies are in phase with the climatological mean wave 1 in February, implying that the sea-ice loss could lead to an amplification of wavenumber-1 baroclinic wave, consistent with the results in previous studies^{1,13}. A Plumb flux analysis also reveals that more upward baroclinic waves on timescales of 2.5–6 days over the BKS propagate into the stratosphere (Fig. 3e,f) due to the weaker static stability in the middle and upper troposphere (Supplementary Fig. 4c,d) during the low-SIC years than during the high-SIC years. Anomalous active wavenumber-1 planetary waves in the stratosphere could push the Arctic vortex towards the Eurasian continent²³ and favour a vortex displacement event^{24,25}. In addition, the lower geopotential height at 50 hPa over the Eurasian continent induces a cyclonic flow (Fig. 3c,d) in the low-SIC years compared to the high-SIC years, leading to positive PV anomalies in the UTLS, and intensifies the shift of the vortex edge towards the Eurasian continent. Recall that there is lower SIC during the 2000s than the 1980s; hence, the polar vortex in late winter shifts to the Eurasian continent over the recent decade.

Over the past three decades, the increased snow cover over the Eurasian continent during autumn and winter was increasingly associated with the ‘Arctic amplification’²⁶. The potential influence

of the increased Eurasian snow cover on the position of the polar vortex is also worth investigation. The surface albedo over the Eurasian continent (37.5°–57.5° N, 20°–135° E) derived from Satellite Application Facility on Climate Monitoring (CM-SAF) data shows a 3.2% increase during autumn and winter for the period 1982–2009. Therefore, we conducted a numerical experiment R5 with the Eurasian surface albedo increased by 5% in the autumn and winter months (see Methods). Supplementary Fig. 6a shows that the geopotential heights near the surface over the Eurasian continent in R5 are lower than in R1 since the surface with a higher albedo in R5 reflects more short-wave radiation away from the surface and the temperature falls. Under the influence of ‘warm Arctic–cold continents’ pattern^{27,28}, there are positive height anomalies to the north of the Eurasian continent. The increased Eurasian snow cover also leads to the amplification of wavenumber-1 planetary waves in the lower stratosphere (Supplementary Fig. 6b), similar to the responses to Arctic sea-ice loss. Accordingly, the edge of the polar vortex also shows a shift towards the Eurasian continent in R5 compared with that in R1 (Fig. 2d). However, it should be pointed out that the responses to snow cover increases are not exactly the same as those to sea-ice loss—particularly at 850 hPa, where the height responses to snow cover increases and sea-ice loss are quite different (Supplementary Fig. 6a).

To provide more insight into the influence of the polar vortex position changes on the Northern Hemisphere surface climate, the PV averaged over Siberia (60°–75° N, 60°–90° E, hereafter referred to as ‘SPV index’) between the isentropic layer 430–600 K is analysed. Note that the shift of the polar vortex towards the Eurasian

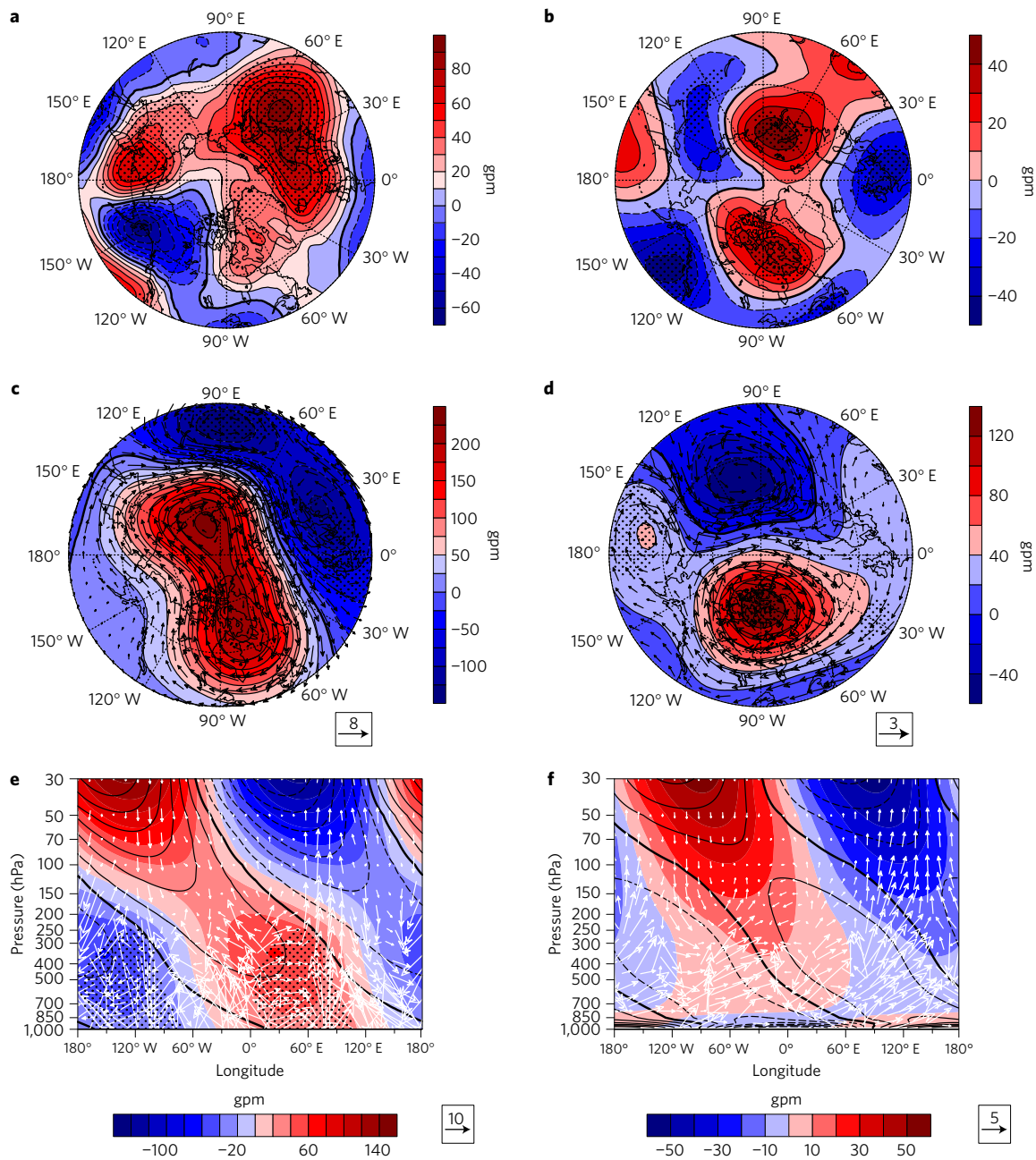


Figure 3 | Analysis of meteorological fields. **a, c**, February mean differences between the BKS low- and high-SIC years in geopotential height at 850 hPa (**a**) and 50 hPa (**c**) (colour-filled and contour lines), with horizontal wind (vectors) at 50 hPa also shown in **c**. **e**, Height-longitude cross-section along 60° N of zonal wave-1 geopotential height anomalies (colour-filled contours) and vertical component of Plumb flux on timescales of 2.5–6 days (vectors). The climatological mean of zonal wave-1 geopotential height anomalies along 60° N for the period 1980–2009 (contour lines) is also shown in **e**, **b, d, f**. As in **a, c, e**, respectively, but for the WACCM-simulated differences between R2 and R1. The climatological mean of zonal wave-1 geopotential height anomalies along 60° N in R1 is also shown in **f**. The differences over the dotted regions are statistically significant at the 90% confidence level according to the Student's *t*-test. The solid and dashed lines in **e** and **f** represent the positive and negative values, respectively.

continent could cause PV increases over Siberia (Fig. 1a). Figure 4a,b indicates that there are low-pressure anomalies accompanied by more than 3 K cooling over the Eurasian continent in February associated with the vortex shift. We estimated that the contribution of stratospheric polar vortex shift on the Siberian cooling is about 10% (the blocking over the upstream region of Siberia can account for 36% of the Siberian cooling in February, see Supplementary Information I). In March, based on the composite differences between high and low SPV, the vortex shift in February could lead to an increase in surface temperature over the northeastern Asian continent and up to -3 K temperature anomalies over northeastern

Canada. Note that the changes in the surface temperature are closely related to the barotropic Rossby wave trains in the middle and upper troposphere, that is, positive (negative) height anomalies and anomalously high (low) pressure correspond to warming (cooling) anomalies (Fig. 4). These Rossby wave trains are induced by the intrusion of high PV air induced by the vortex shift towards Siberia (Supplementary Fig. 8a). The simulations from a linearized barotropic vorticity equation model (see Methods) support the notion that the high vorticity perturbations over the Siberian region (Supplementary Fig. 8e) can produce barotropic Rossby wave trains from Asia to the American continent (Supplementary Fig. 8f) and

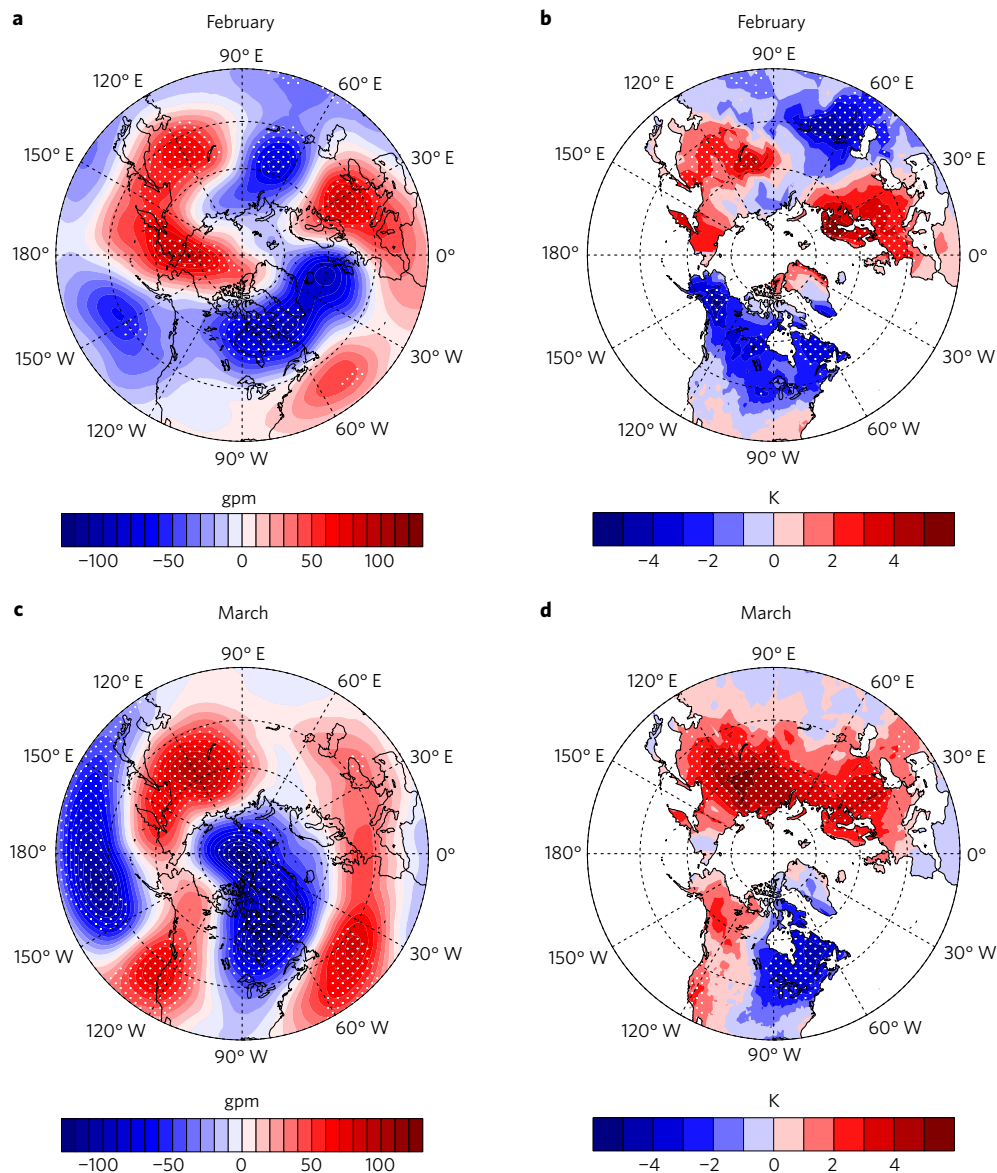


Figure 4 | Impact of the polar vortex shift. a–d. Composite differences in geopotential height at 500 hPa (**a,c**) and surface temperature (**b,d**) in February and March between high and low February-mean SPV index. The composited differences over the dotted regions are statistically significant at the 90% confidence level according to the Student's *t*-test.

then change the tropospheric temperatures over the Eurasian and American continents in March. Apart from the above mechanism, it seems that effects of the polar vortex shift on the surface temperature are also intimately linked to tropospheric blockings. However, the influences are not necessarily related to sudden stratospheric warming (SSW) events, since the definition of vortex edge is based on a well-defined vortex. It should be pointed out that the internal tropospheric climate variability²⁹ and strengthened Ural high due to the sea-ice loss^{4,30} may also contribute to the cooling anomalies over Eurasia.

In summary, our analysis suggested that the vortex shift towards Eurasia could lead to a cooler climate over some parts of the continents during late winter and early spring, which may partly offset the climate warming in these seasons. Under the scenario of persistent sea-ice loss due to global warming in the future^{6,7}, the potential polar vortex shift and its associated climatic influences deserve public attention. As a final remark, other factors, such as polar stratospheric ozone depletion and AO, may also have impacts on the vortex position and these issues are worth further investigation.

Methods

Methods and any associated references are available in the [online version of the paper](#).

Received 22 December 2015; accepted 26 August 2016;
published online 24 October 2016

References

- Kim, B. M. *et al.* Weakening of the stratospheric polar vortex by Arctic sea-ice loss. *Nat. Commun.* **5**, 4646 (2014).
- Alexeev, V. A., Esau, I. N., Polyakov, I. V., Byam, S. J. & Sorokina, S. Vertical structure of recent Arctic warming from observed data and reanalysis products. *Climatic Change* **111**, 215–239 (2011).
- Cohen, J. *et al.* Recent Arctic amplification and extreme mid-latitude weather. *Nat. Geosci.* **7**, 627–637 (2014).
- Mori, M., Watanabe, M., Shiogama, H., Inoue, J. & Kimoto, M. Robust Arctic sea-ice influence on the frequent Eurasian cold winters in past decades. *Nat. Geosci.* **7**, 869–873 (2014).
- Francis, J. A. & Vavrus, S. J. Evidence linking Arctic amplification to extreme weather in mid-latitudes. *Geophys. Res. Lett.* **39**, L06801 (2012).

6. Boe, J. L., Hall, A. & Qu, X. September sea-ice cover in the Arctic Ocean projected to vanish by 2100. *Nat. Geosci.* **2**, 341–343 (2009).
7. Liu, J. P., Song, M. R., Horton, R. M. & Hu, Y. Y. Reducing spread in climate model projections of a September ice-free Arctic. *Proc. Natl Acad. Sci. USA* **110**, 12571–12576 (2013).
8. IPCC *Climate Change 2013: The Physical Science Basis* (eds Stocker, T. F. *et al.*) (Cambridge Univ. Press, 2013).
9. Stroeve, J., Holland, M. M., Meier, W., Scambos, T. & Serreze, M. Arctic sea ice decline: faster than forecast. *Geophys. Res. Lett.* **34**, L09501 (2007).
10. Perovich, D. K. & Richter-Menge, J. A. Loss of sea ice in the Arctic. *Annu. Rev. Mar. Sci.* **1**, 417–441 (2009).
11. Alexander, M. A. *et al.* The atmospheric response to realistic Arctic sea ice anomalies in an AGCM during winter. *J. Clim.* **17**, 890–905 (2004).
12. Deser, C., Tomas, R. A. & Peng, S. L. The transient atmospheric circulation response to North Atlantic SST and sea ice anomalies. *J. Clim.* **20**, 4751–4767 (2007).
13. Peings, Y. & Magnusdottir, G. Response of the Wintertime Northern Hemisphere atmospheric circulation to current and projected Arctic sea ice decline: a numerical study with CAM5. *J. Clim.* **27**, 244–264 (2014).
14. Sun, L., Deser, C. & Tomas, R. A. Mechanisms of stratospheric and tropospheric circulation response to projected Arctic sea ice loss. *J. Clim.* **28**, 7824–7845 (2015).
15. Scinocca, J. F. *et al.* Impact of sudden Arctic sea-ice loss on stratospheric polar ozone recovery. *Geophys. Res. Lett.* **36**, L24701 (2009).
16. Screen, J. A., Simmonds, I., Deser, C. & Tomas, R. The atmospheric response to three decades of observed Arctic sea ice loss. *J. Clim.* **26**, 1230–1248 (2013).
17. Sun, L. T., Deser, C., Polvani, L. & Tomas, R. Influence of projected Arctic sea ice loss on polar stratospheric ozone and circulation in spring. *Environ. Res. Lett.* **9**, 8 (2014).
18. Ambaum, M. H. P. & Hoskins, B. The NAO troposphere–stratosphere connection. *J. Clim.* **15**, 1969–1978 (2002).
19. Mitchell, D. M., Gray, L. J., Anstey, J., Baldwin, M. P. & Charlton-Perez, A. J. The influence of stratospheric vortex displacements and splits on surface climate. *J. Clim.* **26**, 2668–2682 (2013).
20. Seviour, W. J. M., Mitchell, D. M. & Gray, L. J. A practical method to identify displaced and split stratospheric polar vortex events. *Geophys. Res. Lett.* **40**, 5268–5273 (2013).
21. O’Callaghan, A., Joshi, M., Stevens, D. & Mitchell, D. The effects of different sudden stratospheric warming types on the ocean. *Geophys. Res. Lett.* **41**, 7739–7745 (2014).
22. Cohen, J. L., Furtado, J. C., Barlow, M., Alexeev, V. A. & Cherry, J. E. Asymmetric seasonal temperature trends. *Geophys. Res. Lett.* **39**, L04705 (2012).
23. Harvey, V. L., Pierce, R. B., Fairlie, T. D. & Hitchman, M. H. A climatology of stratospheric polar vortices and anticyclones. *J. Geophys. Res.* **107**, 4442 (2002).
24. Charlton, A. J. & Polvani, L. M. A new look at stratospheric sudden warmings. Part I: climatology and modeling benchmarks. *J. Clim.* **20**, 449–469 (2007).
25. Mitchell, D. M., Charlton-Perez, A. J. & Gray, L. J. Characterizing the variability and extremes of the stratospheric polar vortices using 2D moment analysis. *J. Atmos. Sci.* **68**, 1194–1213 (2011).
26. Cohen, J., Furtado, J., Barlow, M., Alexeev, V. & Cherry, J. Arctic warming, increasing fall snow cover and widespread boreal winter cooling. *Environ. Res. Lett.* **7**, 014007 (2012).
27. Overland, J. E., Wood, K. R. & Wang, M. Y. Warm Arctic–cold continents: climate impacts of the newly open Arctic Sea. *Polar Res.* **30**, 15787 (2011).
28. Cohen, J., Jones, J., Furtado, J. C. & Tziperman, E. Warm Arctic, cold continents a common pattern related to Arctic sea ice melt, snow advance, and extreme winter weather. *Oceanography* **26**, 152–160 (2013).
29. Sun, L., Perlwitz, J. & Hoerling, M. What caused the recent “Warm Arctic, Cold Continents” trend pattern in winter temperatures? *Geophys. Res. Lett.* **43**, 5345–5352 (2016).
30. Kug, J. S. *et al.* Two distinct influences of Arctic warming on cold winters over North America and East Asia. *Nat. Geosci.* **8**, 759–762 (2015).

Acknowledgements

This work is supported by the National Science Foundation of China (41225018, 41575038). This work is also supported by the Foundation for Innovative Research Groups of the National Science Foundation of China (Grant No. 41521004). We thank S.-W. Son for comments and suggestions. Matlab codes for the linearized barotropic vorticity equation model support provided by J. Shaman and E. Tziperman are highly appreciated. We thank the scientific teams for ECMWF, NASA, Hadley Centre, CM SAF data and CMIP5 multi-model data. We also thank NCAR for providing the WACCM3 model.

Author contributions

J.Z. and W.T. contributed to writing the paper, design of the numerical experiments and data analysis. M.P.C. contributed to the discussion and writing the paper. F.X. contributed to the discussion and design of the numerical experiments. J.H. contributed to the data analysis. All authors reviewed the manuscript.

Additional information

Supplementary information is available in the [online version of the paper](#). Reprints and permissions information is available online at www.nature.com/reprints. Correspondence and requests for materials should be addressed to W.T.

Competing financial interests

The authors declare no competing financial interests.

Methods

Data sets. The ERA-Interim data used here has a horizontal resolution of 1° (latitude) \times 1.25° (longitude) and has 17 isentropic levels and 37 pressure levels. The NASA-MERRA data set is also used to analyse the polar vortex edge and temperature. We have vertically interpolated the MERRA data fields onto the isentropic coordinate of the ERA-Interim data. The sea-ice concentration (SIC) and sea surface temperature (SST) are derived from the monthly Sea Ice and Sea Surface Temperature data set from the Hadley Centre, in which sea ice is retrieved from various sources of digitized sea-ice charts and passive microwave imagery³¹.

Polar vortex analysis. The vortex edge is defined as the location of the largest Ertel potential vorticity (EPV) gradient, with an additional constraint of close proximity to a strong westerly jet, according to the method of Nash and colleagues³². The monthly mean vortex edge is not calculated when the polar vortex breaks up or if the shape of vortex is not well defined, usually when the duration of major sudden stratospheric warming (SSW) events occurring in this month exceeds 15 days. Such major SSW events occurred in February during 1987, 2006, 2009 and 2013. The daily mean vortex edge is also not calculated during the major SSW events. In addition, we defined the location of the maximum value of the PV averaged between the layers 430–600 K as the vortex centre.

Composite analysis. The composites during the high- and low-SIC years are calculated when the detrended and 6-month (September–February) mean SIC over the BKS (70° – 90° N, 0° – 90° E) is greater and less than 1 and -1 standard deviation, respectively. The composited differences for a given field are calculated by averaging the detrended monthly mean field during the low-SIC years minus that during the high-SIC years. The two-tailed Student's *t*-test is used to calculate the statistical significance of the composite differences.

Model and simulations. The Whole Atmosphere Community Climate Model, version 3 (WACCM3) has 66 vertical levels extending from the ground to 145 km, with a vertical resolution of 1.1–1.4 km near the tropopause region. The time-slice simulations presented in this paper were performed at a resolution of 1.9° (latitude) \times 2.5° (longitude), with interactive chemistry disabled and the quasi-biennial oscillation (QBO) turned off. The control experiment (R1) was performed with a seasonal cycle of SIC and SST based on the decadal mean of the Hadley Centre SIC and SST in the 1980s. In experiment R2, the SST is the same as in R1, except that

the SIC forcing represents the decadal mean of the SIC during the 2000s when the sea ice is reduced. Simulations R1 and R2 use the same greenhouse gas emissions and the same climatology of ozone for the period 1980–2009. The experiments R1 and R2 were run for 25 years with the first 5 years excluded for model 'spin-up'; the remaining 20 years of output is used for the analysis. Two additional experiments (R3 and R4) were performed with six ensemble members. Each ensemble run was run for 15 years with the first 5 years excluded for model 'spin-up'; the remaining 10 years of model data from each ensemble run is used for the analysis. The control experiment (R3) was performed with the same seasonal varying SIC and SSTs in the 1980s as those in R1. In the perturbed run (R4), the SSTs and SIC are the same as those in R3, except that the sea ice over the BKS from September to February are replaced with corresponding sea-ice climatologies in the 2000s. The experiments R3 and R4 are designed to analyse the influence of sea-ice loss over the BKS in autumn and winter on the vortex shift. The experiment R5 was conducted to analyse the influence of Eurasian snow cover changes on the polar vortex shift. The SIC and SSTs of R5 are the same as those in R1, except that the surface albedo over the Eurasian continent (37.5° – 52.5° N, 20° – 135° E) during autumn and winter in R5 is 5% higher than that in R1.

A linearized barotropic vorticity equation model (LBM) is used to investigate how the PV changes over Siberia associated with the vortex shift influence the Northern Hemisphere surface temperatures through Rossby wave trains. The LBM is based on the steady, forced barotropic vorticity equation:

$$J(\psi, \nabla^2 \psi + f) + \alpha \nabla^2 \psi + K \nabla^4 (\nabla^2 \psi) = R$$

where ψ is the stream function, f is the Coriolis parameter, R is a forcing function, α of $1.57 \times 10^{-6} \text{ s}^{-1}$ is the Rayleigh coefficient, K is equal to $2.34 \times 10^6 \text{ m}^4 \text{ s}^{-1}$, and the Jacobi function $J(A, B) = (1/a^2 \cos \phi)((\partial A/\partial \lambda)(\partial B/\partial \phi) - (\partial A/\partial \phi)(\partial B/\partial \lambda))$ with latitude ϕ , longitude λ and Earth's radius a .

References

- Rayner, N. A. *et al.* Global analyses of sea surface temperature, sea ice, and night marine air temperature since the late nineteenth century. *J. Geophys. Res.* **108**, 4407 (2003).
- Nash, E. R., Newman, P. A., Rosenfield, J. E. & Schoeberl, M. R. An objective determination of the polar vortex using Ertel's potential vorticity. *J. Geophys. Res.* **101**, 9471–9478 (1996).